KECK Geology Consortium
Learning Science Through Research
Published by the Keck Geology Consortium
Short Contributions
Keck Geology Consortium
Volume 34
May 2022
doi: 10.18277/AKRSG.2022.34.08

ASSESSING THE IMPACT OF SOIL ON MANGANESE CONTAMINATION IN SPRINGS AND GROUNDWATER IN THE SHENANDOAH VALLEY, VIRGINIA

HALEY CULBERTSON, Washington & Lee University
Project Advisor: Margaret A. G. Hinkle

INTRODUCTION

There are multiple potential geogenic and anthropogenic sources of Mn in surface water and groundwater. Since the discovery of manganese (Mn) in 1774 (Weeks, 1932), it has been utilized for a plethora of purposes in American industry, including infrastructure and agriculture (Johnson, 2006). Mn has also been mined for energy production and fertilizer for decades, the byproducts of which all contribute to Mn entering waterways (Howe and International Programme on Chemical Safety, 2004). In the Blue Ridge Mountains, geogenic sources of Mn are hypothesized to have existed since the Paleozoic era (Pegau, 1958) as a result of clay weathering processes at the contact of the Shady Dolomite and Erwin Formations, forming primarily Mn(III/IV) oxide minerals such as pyrolusite and hollandite (Carmichael et al., 2017; Stose et al., 1919). To the west in the Shenandoah Valley, the origin of Mn ores is thought to be a two-step process involving hydrothermal deposition followed by supergene enrichment. In other words, Mn(III/IV) oxides initially precipitated from a hot solution of mineral enriched water which forced its way through cracks in the Earth's surface, followed by supergene alteration from the downward percolation of mineral- bearing surface water, as evidenced by two distinct mineralogies and geochemical signatures (Carmichael et al., 2017). South of the Shenandoah Valley in the Roanoke River Watershed, Mn ores are believed to have been formed by only supergene processes, with temperatures below 130°C, as indicated by the presence of goethite (Kiracofe et al., 2017). However, rather than a strictly downward percolation model as previously hypothesized (Espenshade, 1954). Kiracofe et al. (2017) suggests Mn was first released from country rock via chemical weathering and carried to reducing conditions by downward percolating groundwater where it was then trapped in mineral structures due to diagenesis and metamorphism. This process is believed to have been followed by the upwelling of anoxic groundwater, releasing $Mn(II)_{aq}$ by chemical weathering, which was then transported to oxic conditions with sufficient microbial support to precipitate Mn(III/IV) oxides (Kiracofe et al., 2017). In all cases, these Mn (oxyhydr)oxide deposits weather and erode through time, transported by aeolian and alluvial processes to eventually end up in the water system.

Because Mn speciation is largely dependent on environmental conditions, with suboxic and anoxic conditions promoting $Mn(II)_{aq}$, drinking water obtained from groundwater sources is of particular concern. Groundwater resources are incredibly relied upon throughout the Shenandoah Valley, as a large percentage of inhabitants rely on springs and groundwater wells as their main source of drinking water (USGS, 2022). Additionally, a redox disequilibrium exists at springs (where the saturated zone meets the topographic surface) as anoxic or suboxic groundwater meets the oxygen-rich surficial environment, encouraging $Mn(II)_{aq}$ to oxidize to Mn(III/IV) oxides. This work investigates the role of soils on Mn concentrations in both springs and groundwater wells throughout the Shenandoah Valley, VA through Mn K-edge X-ray adsorption near-edge structure (XANES) spectroscopy and scanning electron microscopy with energy dispersive X-ray spectroscopy (SEM/EDS).

METHODS AND MATERIALS

Field Sites

The study area of this project consists of four counties across the Shenandoah Valley, including Rockbridge, Augusta, Bath and Shenandoah. The region is characterized by rural mountain landscapes, with historical cities distributed throughout, containing a total population of 145,659. A total of 24 springs (Fig. 1) were selected for sampling based on accessibility, permission, and regions of interest identified from groundwater well data from the Virginia Household Water Quality Project (VAHWQP).

Rockbridge County Sampling Sites

In Rockbridge County, Pond Spring (PS) is currently used to feed a pond that serves as the focal point of an outdoor event center. The spring itself is classified as a seep and located on the west side of the pond, the two slightly separated by a dirt mound covered by grasses, through which water flows. The pond directly east of the mound was a murky white on the day of sampling, possibly due to chemical treatments, but most likely due to decaying organisms (Aswiyanti et al., 2021). Kerr's Creek (KC) is a gaining stream upstream of PS with springs contributing to its flow.

Augusta County Sampling Sites

In Augusta County, Bubbling Springs (BUBS) and Augusta Springs and Wetlands (AWS) are located in the George Washington and Jefferson National Forests. BUBS is a spring-fed pond and is characterized by bubbles believed to be CO_2. The pond bottom is full of yellow, red, black, green, and brown pebbles and the water is extremely clear. In contrast, AWS is a complex of seeps, springs, and creeks. The area has been slightly developed with parking and picnic areas, as well as several post-colonial structures including a spring house, bottling plant foundations, and a hypothesized root cellar.

Disappearing Ponds Complex

Finally, also located within Augusta County and the George Washington and Jefferson National Forests, is the Maple Flats Ponds complex, a series of clay bottom ponds (Fleming and Alstine, 1999). Four of these ponds were included in this study: Frog/Oak Pond (FOP), located nearest to a relict Mn ore mine, Twin Ponds (TPS/N), Deep Pond (DP), and Spring Pond (SP), the latter being the largest and only pond never observed to dry up, and is likely spring-fed. All the ponds contained some water at the time of sampling (August 2021), but exact depth could not be determined because the soft clay bottom prevented wading into the centers. Other than SP, which was surrounded by tall, dense grasses and fruit bushes, the ponds were not dramatically different in appearance from one another. Most have no apparent input or output of water with the exception of precipitation and evaporation. This site was selected as a means to isolate Mn derived from soil weathering versus Mn inputs from groundwater.

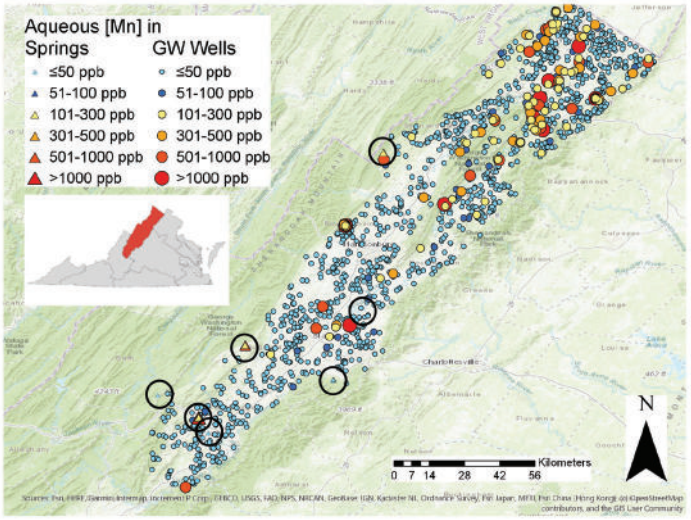

Figure 1. Map of aqueous Mn concentrations in springs (triangles) and groundwater wells (circles) in the Shenandoah Valley, VA, with increasing concentrations increasing the relative size of each data point based on demarcations from ≤50 ppb (light blue) to 51-100 ppb (dark blue) to 101-300 ppb (yellow; above which low level chronic exposure to Mn via drinking water may result in health effects), 301-500 ppb (orange), 501-1000 ppb (light red), to >1000 ppb (dark red). Field sites for springs and seeps are denoted with black circles.

Shenandoah County

The unincorporated town of Shrine Mont (SM) in Shenandoah Co. hosts multiple springs which have undergone over a century of documented use. Because of their history of use, each of the springs, three in total, had some sort of spring house structure built around them out of either wood or stone, with metal pipes used to bring the water to the surface. These

springs included Shrine Mont Orkney Spring (SMOS), Bear Wallow Spring (SMBW), and Tea Spring (SMTS). With the exception of SMBW, extensive Fe oxidation was visible in the form of bright red precipitates coating rocks surrounding the areas.

Soil Analyses

To determine the general composition of the soil samples, small amounts of each sample were mounted to aluminum stubs with double-sided carbon paper for SEM/EDS. These analyses provided elemental distributions and morphologic features across soils and determined the prioritization of samples for XANES spectroscopy. In total, samples analyzed with XANES spectroscopy include AWS03A, KC01A, KC02A, FOP01A, DP01A, and PS02. The "top" and "bottom" of each core was determined by either distinguishable differences in horizon by color or at least 3 cm from the respective end of the core.

Samples and Mn oxidation state standards were analyzed at beamline 12-BM-B, which uses a Si(111) fixed offset double-crystal monochromator with a toroidal focusing and flat harmonic rejection mirrors. XANES spectra of the Mn metal foil were collected at the beginning, end, and multiple mid points to calibrate the monochromators to 6539 eV, the Mn K-edge. Linear combination fits (LCFs) using a suite of XANES spectra standards [manganese (II) chloride [$MnCl_2$], rhodochrosite [$MnCO_3$], manganese (II) sulfate [$MnSO_4$], hausmannite [$Mn(II/III)_2O_4$], bixbyite [Mn,Fe_2O_3], manganite [MnO], feitknechtite [Mn(III)O(OH)], pyrolusite [MnO_2], ramsdellite [MnO_2], KBi, and calcium manganese oxide [$Ca_2Mn_3O_8$], with Mn(IV) standards from Manceau et al. (2012)] determined the average Mn oxidation state (AMOS) of the select soil samples, as well as the fraction of Mn(II/III/IV)s. These LCFs and the total concentration of Mn in the samples determined by XRF from Willis (2022) were used to calculate the actual concentration of Mn(II/III/IV)s per sample.

Total soil moisture content was determined via gravimetric analysis. Soil pH was determined by combining up to 5.0 g of soil with 10 mL of 0.1 M $CaCl_2$. These solutions were mixed with a glass rod and allowed to settle for >30 minutes before the separated solution pH was measured.

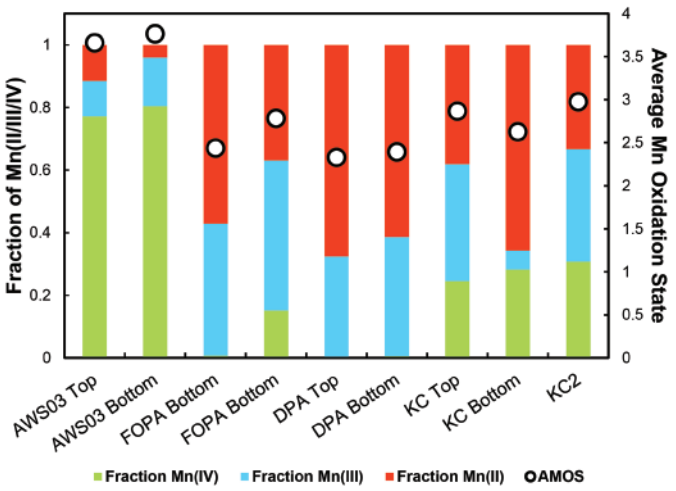

Figure 2. The fractions of Mn(IV) (green), Mn(III) (blue), and Mn(II) (red) and average Mn oxidation state (AMOS; white circles with black outlines) obtained by LCFs for each sample analyzed by Mn K-edge XANES spectroscopy.

RESULTS

Average Mn Oxidation State (AMOS) of Soils of Interest

Substantial Mn(II) (>10%) was found in every sample analyzed by XANES spectroscopy, in varying proportions (Figure 2). Comparing samples within the field sites, the AMOS determined was relatively similar, a trend that was also found within the individual cores. Every soil sample has an AMOS between 2.0 and 4.0, with the exception of PS, whose XANES spectra exhibits a white line at surprisingly high energy beyond all of the Mn(IV) standards and consistent with Mn(VII) (Figure 3). A sample from AWS, AWS03A, exhibits the highest fraction of Mn(IV) with Mn(II/III) comprising just 20-30% (Table 1). In most soil cores, the AMOS is slightly higher in the bottom of the core than the top, similar to Gillispie et al. (2016) which found that the weathering of Mn bearing soils in the Piedmont region of North Carolina contribute to Mn contamination in shallow groundwater wells, with Mn(II/III) minerals near the surface and Mn(III/IV) oxide minerals at depth. There is an exception to this trend in KC01A (Fig. 2), with an AMOS of 2.87 at the top and that of 2.63 at the bottom. KC01A is particularly notable due to the extremely high soil Mn in the bottom of the core and lack of soil Mn in the top (Table 1) and the fact that it is the one sample near a stream rather than a spring/seep.

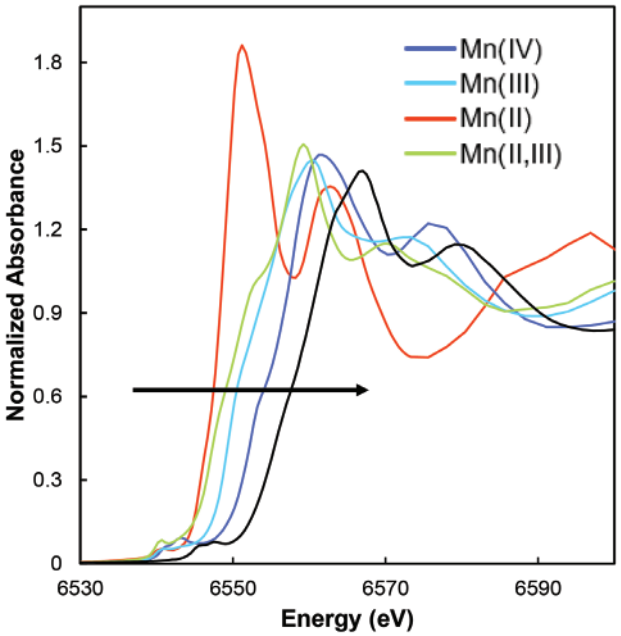

Figure 3. XANES spectra of example Mn oxidation state standards for each oxidation state used for LCFs, with Mn(IV) (dark blue), Mn(III) (light blue), Mn(II/III) (green), and Mn(II) (red) showing the progressive shift toward higher energy with increasing Mn oxidation state, compared with the sample spectra for PS (black). The sample spectra for PS is clearly shifted substantially toward higher energy, beyond that of Mn(IV) standards, indicating its oxidation state is higher than what is normally observed in soil environments.

Paired with the total soil [Mn] determined by XRF, the actual concentration of Mn(II/III/IV) for each sample was calculated (Table 1). Substantial concentrations of soil Mn(IV) were found in cores AWS03A and KC samples. Soil Mn was below the limit of detection for sample FOP01A bottom and the entire DP01A core. Other than these samples, every sample was found to have relatively high concentrations of soil Mn (Table 1) compared to the USGS soils map of the US (Smith et al., 2019).

Relationship Between Mn in Soils and Mn_{aq}

Plotting aqueous Mn in nearby waters vs AMOS and the fractions of Mn(II/III/IV) yields interesting trends. The site-averaged AMOS of soils and $[Mn]_{aq}$ display an inverse relationship ($R^2 = 0.44$), as also occurs for Mn(IV) and $[Mn]_{aq}$ ($R^2 = 0.49$) (Figure 4). When a soil sample has an AMOS closer to 4.0, the spring water collected has a concentration between 0.00 and 5.00 ppm; but when a soil sample has an AMOS closer to 2.0, the corresponding spring water sample $[Mn]_{aq}$ increases substantially. It should be noted that all samples analyzed by XANES spectroscopy happened to have lower aqueous Mn (aside from PS which was removed from this portion of the analysis due to its AMOS of ~+7), thus the maximum aqueous Mn in this data set is just 35 ppm, likely in part because these samples were selected based on observable soil Mn, and higher soil Mn corresponds with lower aqueous Mn.

Soil Mn(II) and $[Mn]_{aq}$ are directly related to one another, with a greater fraction of Mn(II) in soils correlating with higher $[Mn]_{aq}$ in corresponding spring waters ($R^2 = 0.36$). While most commonly existing in oxide minerals and thus usually expected to behave similarly to Mn(IV), Mn(III) also shows a negative correlation relationship with $[Mn]_{aq}$ ($R^2 = 0.60$) (Figure 4).

Table 1. Total soil Mn concentrations, fractions of soil Mn(II/III/IV) and corresponding average Mn oxidation states (AMOS) and actual concentrations of soil-associated Mn(II/III/IV), along with general soil parameters (percent organic matter (OM), percent total organic carbon (TOC), pH, and approximate percentages of sand, silt, and clay based on textural analyses.

Sample	Total [Mn]s (ppm)	fMn(IV)s	f Mn(III)s	fMn(II)s	[Mn(II)]s (ppm)	[Mn(III)]s (ppm)	[Mn(IV)]s (ppm)	[Mn]aq (ppb)	% OM	% TOC	pH	% Clay	% Sand	% Silt	Other Major and Trace Metals Present in Soils
AWS03A-top	1,225	0.77	0.11	0.11	140	139	946	0.90	8%	13%	6.0	35%	10%	55%	Zn,Fe, Cr, Ni, Pb, Ti, Zr
AWS03A- bottom	2,058	0.80	0.16	0.04	84	320	1,655	0.90	9%	16%	6.0	25%	65%	15%	Zn,Fe, Cr, Ni, Pb, Ti, Zr
FOPA- top	176	0.01	0.42	0.57	100	74	1	34.80	7%	13%	5.0	45%	10%	45%	Fe, Pb, Ti, Zn
FOPA- bottom	-	0.15	0.48	0.37	-	-	-	34.80	4%	7%	4.6	45%	5%	50%	Zr, Fe, Cr, Ti,
DP01A- top	-	0.00	0.32	0.68	-	-	-	10.50	8%	13%	4.0	45%	50%	5%	Fe, Ti
DP01A- bottom	-	0.01	0.38	0.61	-	-	-	10.50	1%	3%	3.5	30%	50%	20%	Fe, Ti
KC01A- top	415	0.25	0.37	0.38	158	155	102	9.60	3%	6%	5.6	5%	90%	5%	Fe, Cr, Ni, Ti
KC01A- bottom	17,801	0.28	0.06	0.66	11,698	1,067	5,037	9.60	5%	9%	6.0	0%	100%	0%	Ti, Fe, Cr, Ni, Zr
KC02A	23,754	0.31	0.36	0.33	7,910	8,544	7,300	9.60	4%	7%	6.2	10%	60%	30%	Zr, Fe, Ti, Sn, Cr
PS02A- top	9,301	-	-	-	-	-	-	173-1322	-	-	3.9	-	-	-	-
PS02A- Bottom	12,659	-	-	-	-	-	-	173-1322	-	-	3.1	-	-	-	-

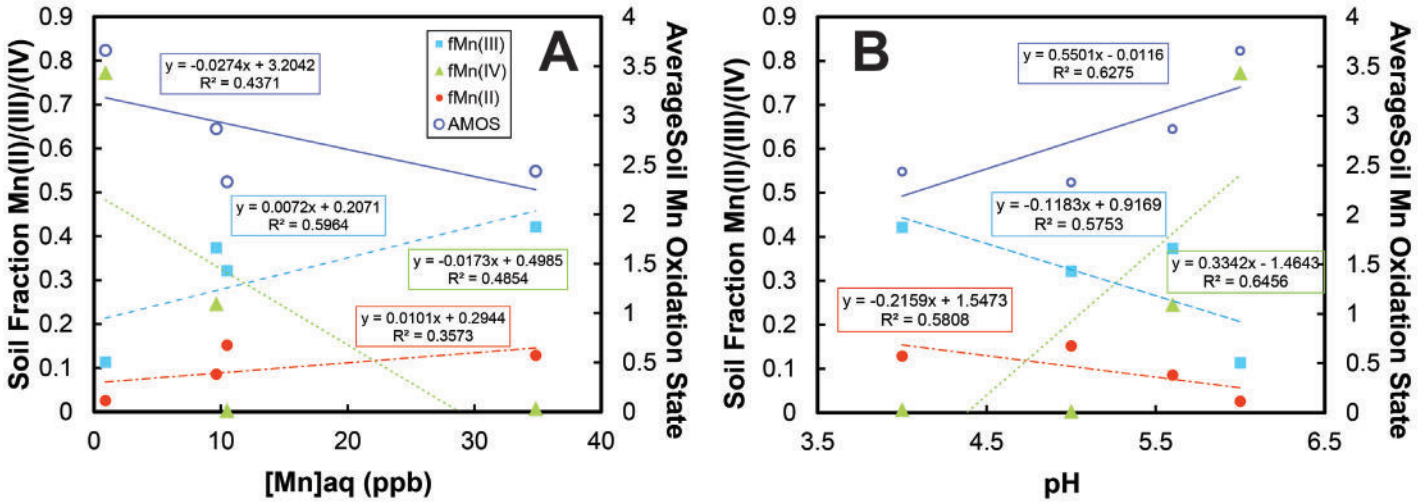

Figure 4. Fraction of Mn(IV) (green triangles), Mn(III) (light blue squares), and Mn(II) (red circles) in soils as well as the AMOS (white circles with blue borders) as a function of aqueous Mn concentrations in nearby springs and seeps (A) and of pH (B).

Soil Characteristics and AMOS Trends

Most of the soils sampled (28/52) contained 50% or greater sand, while the next most common soil component was clay (21/52 samples with greater than 50%), with only 3 samples composed of majority silt (Table 1). Only two cores, both collected from Rockbridge County, have a pH ≥ 7.0, with the other 48 samples being acidic. Soils with confirmed Mns were found to be acidic, with pH levels consistently less than or equal to 6.0 (Table 1). These soils also have very high proportions of silt in comparison to the rest of the samples, with the exception of one sample from Shenandoah County (Table 1). Site averaged AMOS and the fraction of Mn(IV) in samples show a directly correlated relationship with increasing pH, while the fraction of Mn(II) and (III) both show inverse relationships ($R^2 > 0.57$) (Figure 4). These trends are consistent with those shown between the fraction of Mn(II/III/IV) and $[Mn]_{aq}$ in spring waters.

Heavy Metals Associated with Mn_s

Soils which were prioritized for XANES were analyzed with SEM/EDS for a second time, more thoroughly, to determine elemental associations with soil Mn_s. During these analyses, Mns was found as precipitates on other grains without defined boundaries and as distinguishable grains with definitive platy geometry. In every sample, regardless of perceived Mns morphology, Mn was associated with various heavy metal contaminants including chromium (Cr), nickel (Ni), and lead (Pb) (Table 1). Also consistently associated with Mns in soils were Fe and titanium (Ti).

DISCUSSION

Across the Shenandoah Valley, previously analyzed groundwater wells show two contamination "hotspots" (McMahon et al., 2018). Including data from the VAHWQP broadened our groundwater well network to >1,900 wells within the Shenandoah Valley and suggests multiple Mn "hotspots", all of which are in agreement with $[Mn(II)]_{aq}$ found in spring waters by this study, with the exception of PS located in central Rockbridge County (Figure 1). Extremely high [Mntotal]soil found by XRF (Table 1) and AMOS greater than 4 (Figure 3), however, indicates that the regular algae treatments given to the pond may likely contain potassium permanganate (KMn7+O4), with Mn(VII) most stable in the aqueous phase. This input of Mn(VII) would also explain the exceptionally elevated $[Mn]_{aq}$ at PS. These remaining hotspots appear to be strongly associated with black shale and sandstone lithologies, while limestone and dolostone lithologies seem to buffer $Mn(II)_{aq}$ contamination of concerning concentrations (>100 ppb). However, the soils found to contain appreciable concentrations of Mns were from sites located outside of these hotspots and are associated with very low spring $[Mn(II)]_{aq}$.

The correlations between the AMOS, Mn(II), and Mn(IV) with$[Mn]_{aq}$ show expected behaviors, confirming that solid-associated Mn(II) is stable in reducing conditions but less so in oxidizing

conditions. The positive correlation between Mn(III)s and $[Mn]_{aq}$, however, seems to contradict these trends (Figure 4A). This relationship may likely be explained by comproportionation reactions that can occur between Mn(II) and Mn(IV) in certain environments where they coexist (Mandernack et al., 1995), generating Mn(III) as follows:

$$Mn(II) + Mn(IV) \leftrightarrow 2Mn(III) \qquad \text{Eq (1)}$$

Thus, increasing $[Mn(II)]_{aq}$ drives the reaction toward generating more Mn(III) (Zhao et al., 2016). These reactions are typically most common in transition zones, such as wetlands, hyporheic zones, and areas contaminated with other heavy metals (McMahon & Chapelle, 2008), which explains the high [Mn(III)] found in soils at AWS and KC (Table 1), which we would classify as hyporheic zones. These results are consistent with McMahon et al. (2018a) findings that groundwater wells closest to surface water bodies are at higher risk for Mn contamination.

Relationships Between Soil Characteristics and AMOS

The trend displayed between Mn(III) in soils and soil pH can likely also be explained by these comproportionation reactions. Although Mn(IV) is seen to decrease with decreasing pH (Figure 4B), because increasingly acidic conditions make $Mn(II)_{aq}$ stable, the reaction would be expected to become more thermodynamically favorable if Mn(IV) were present in the system; however, previous research has shown that decreasing pH inhibited Mn(IV) comproportionation reactions (in pH conditions of 7.4-8.0) (Mandernack et al., 1995). This trend may conversely be interpreted as $Mn(III)_{aq}$ oxidizing to Mn(IV) with increasing pH conditions, which has been found to play a larger role in the system's redox behavior than previously thought (Johnson, 2006).

CONCLUSION

Because of the negative correlation between soil AMOS and $[Mn]_{aq}$, soils which contain Mn(III/IV) oxides appear to have a buffering effect on Mn_{aq} contamination, as the conditions make the reduction reaction of Mn(IV) more unfavorable in terms of both thermodynamics and kinetics. However, common heavy metal associations with potential contaminants such as chromium, nickel, and lead pose the potential risk of mobilizing to groundwater resources if pH or oxidation conditions change. This work finds that $[Mn(II)]_{aq}$ contamination occurs in a spatially distributed manner throughout the Shenandoah Valley, with [Mn]s in nearby soils providing an indication of possible spring and groundwater contamination. While the region is dominated by limestone and dolostone lithologies, providing buffering protection to springs and groundwater wells, the northern Shenandoah Valley is at higher risk due to the greatest proportion of shale and sandstone aquifers in this area.

ACKNOWLEDGEMENTS

This work was supported by the Keck Geology Consortium and the National Science Foundation under Grant No. 2050697. I would specifically like to thank Dr. Margaret Anne Hinkle, my thesis advisor for making this experience manageable, valuable, and fun. Both Dr. Eva Lyon and Emily Falls also deserve huge thanks for their help with field and lab work. Additionally, without the Keck students, and Ani Croy, Noah Wilson, and Chris Goldmann in particular, this project could not have been brought to its current conclusion in less than a year. XANES spectra were collected at beamline 12-BM at the Advanced Photon Source, a U.S. Department of Energy (DOE) Office of Science user facility operated for the DOE Office of Science by Argonne National Laboratory under Contract No. DE-AC02-06CH11357. A huge thanks to Benjamin Reinhart who collected the XANES spectra for this research, as COVID-19 necessitated that XANES spectra were collected with remote user access. This work was additionally supported by the Johnson Opportunity Grant program at Washington and Lee as well as the Washington and Lee Geology Department's Edgar W. Spencer '53 Geology Field Research Fund.

REFERENCES

Aswiyanti, I., Istiqomah, I., Isnansetyo, A., 2021. Isolation and identification of nitrifying bacteria from tilapia (Oreochromis sp.) pond in Sleman Yogyakarta Indonesia. IOP Conf. Ser. Earth Environ. Sci. 919, 012054. https://doi.

org/10.1088/1755-1315/919/1/012054
Carmichael, S.K., Doctor, D.H., Wilson, C.G., Feierstein, J., McAleer, R.J., 2017. New insight into the origin of manganese oxide ore deposits in the Appalachian Valley and Ridge of northeastern Tennessee and northern Virginia, USA. GSA Bull.
David B. Smith, Frederico Solano, Laura G. Woodruff, William F. Cannon, Karl. J. Ellefsen, 2019. USGS Scientific Investigations Report 2017-5118: Geochemical and Mineralogical Maps, with Interpretation, for Soils of the Conterminous United States [WWW Document]. URL https://pubs.usgs.gov/sir/2017/5118/sir20175118_element.php?el=25 (accessed 3.13.22).
Erickson, M.L., Yager, R.M., Kauffman, L.J., Wilson, J.T., 2019. Drinking water quality in the glacial aquifer system, northern USA. Sci. Total Environ. 694, 133735. https://doi.org/10.1016/j.scitotenv.2019.133735
Fleming, G.P., Alstine, N.E.V., 1999. Plant Communities and Floristic Features of Sinkhole Ponds and Seepage Wetlands in Southeastern Augusta County, Virginia. Banisteria 28.
Gilbert H. Espenshade, 1954. Geology and Mineral Deposits of the James River- Roanoke River Manganese District, Virginia. Geol. Surv. Bull. 1008.
Gillispie, E.C., Austin, R.E., Rivera, N.A., Bolich, R., Duckworth, O.W., Bradley, P., Amoozegar, A., Hesterberg, D., Polizzotto, M.L., 2016. Soil Weathering as an Engine for Manganese Contamination of Well Water. Environ. Sci. Technol. 50, 9963–9971. https://doi.org/10.1021/acs.est.6b01686
Howe, P.D., International Programme on Chemical Safety (Eds.), 2004. Manganese and its compounds: environmental aspects, Concise international chemical assessment document. World Health Organization, Geneva.
Johnson, K.S., 2006. Manganese Redox Chemistry Revisited. Science 313, 1896–1897.
Kiracofe, Z.A., Henika, W.S., Schreiber, M.E., 2017. Assessing the Geological Sources of Manganese in the Roanoke River Watershed, Virginia. Environ. Eng. Sci. 23, 43–64.
Mandernack, K.W., Post, J., Tebo, B.M., 1995. Manganese mineral formation by bacterial spores of the marine Bacillus, strain SG-1: Evidence for the direct oxidation of Mn(II) to Mn(IV). Geochim. Cosmochim. Acta 59, 4393–4408. https://doi.org/10.1016/0016-7037(95)00298-E
McMahon, P. b., Chapelle, F. h., 2008. Redox Processes and Water Quality of Selected Principal Aquifer Systems. Groundwater 46, 259–271. https://doi.org/10.1111/j.1745-6584.2007.00385.x
McMahon, P.B., Belitz, K., Reddy, J.E., Johnson, T.D., 2018a. Elevated Manganese Concentrations in United States Groundwater, Role of Land Surface–Soil–Aquifer Connections. Environ. Sci. Technol. 53, 29–38.
McMahon, P.B., Reddy, J.E., Johnson, T.D., 2018b. Data for Elevated Manganese Concentrations in United States Groundwater, Role of Land Surface-Soil-Aquifer Connections. US Geol. Surv. Data Release. https://doi.org/10.5066/P9Y4GOFQ
Pegau, A., 1958. Virginia Manganese Minerals and Ores A Selected Bibliography with Excerpts. Miner. Resour. Circ. 7.
Stose, G.W., Miser, H.D., Katz, F.J., Hewett, D.F., 1919. Manganese Deposits of West Foot of the Blue Ridge Mountains. Va. Geol. Surv. Bull. 17.
USGS, 2022. USGS Current Conditions for Virginia_Groundwater [WWW Document]. URL https://waterdata.usgs.gov/va/nwis/current/?type=gw (accessed 4.12.22).
Weeks, M.E., 1932. The discovery of the elements. III. Some eighteenth-century metals. J. Chem. Educ. 9, 22. https://doi.org/10.1021/ed009p22
Willis, N., 2022. Analysis of Soil Geochemistry to Better Understand Geogenic Manganese Contamination in the Shenandoah Valley. Keck Geology Consortium Short Contributions, 50.
Zhao, H., Zhu, M., Li, W., Elzinga, E.J., Villalobos, M., Liu, F., Zhang, J., Feng, X., Sparks, D.L., 2016. Redox Reactions between Mn(II) and Hexagonal Birnessite Change Its Layer Symmetry. Environ. Sci. Technol. 50, 1750–1758. https://doi.org/10.1021/acs.est.5b04436